Appl. Phys. B 64, 1–13 (1997)

Applied Physics B Lasers and Optics

Invited paper

Fourier-transform heterodyne spectroscopy of liquid and solid surfaces

Doo Soo Chung[1], **Ka Yee Lee**[2], **Eric Mazur**[3]

[1] Department of Chemistry, Seoul National University, Seoul 151-742, Korea
[2] Department of Chemical Engineering, University of California, Santa Barbara, CA 93106-5080, USA
[3] Gordon McKay Laboratory, Harvard University, Cambridge, Massachusetts 02138, USA

Received: 21 August 1996

Abstract. Fourier-transform heterodyne spectroscopy is a simple but powerful technique to study narrow line shapes and small frequency shifts. We review the technique and its application to the study of hydrodynamic fluctuations. We introduce a simple scheme for obtaining the full spectrum of light scattered from liquid and solid surfaces. Using this scheme we obtained a spectral resolution of 200 μHz. Two applications of the technique, one involving the detection of counter-propagating capillary waves, the other measurement of the epitaxial crystal-growth speed of a crystalline silicon interface, are presented.

PACS: 07.65; 68.10; 68.35

In many experiments one is interested in determining changes in a certain physical quantity. This requires measurement of the quantity with respect to a reference value. When it is not possible to measure the quantity directly or to have a reliable reference one can still do accurate *differential* measurements. For example, if one is interested in measuring the small frequency shift of an electromagnetic wave due to a scattering process, one must either measure, to a very high degree of accuracy, the frequencies of each of the incident and scattered waves to determine the frequency difference, or one can measure directly the beat frequency of the two waves. In the second method the difference in frequency of the two waves is directly measured. Differential measurements can be carried out even if the reference (the incident electromagnetic wave) fluctuates and require a smaller relative accuracy than absolute measurements.

In radio and radio-frequency technology differential techniques have been applied extensively. Beating at optical frequencies was first demonstrated in the classic Zeeman splitting experiment of Forrester et al. in 1955 using a mercury lamp as a light source [1]. With the advent of lasers, light-beating spectroscopy has become an important tool for measuring optical lineshapes and small frequency shifts with a resolution on the order of several Hertz [2]. The technique was first used for the study of the output of lasers by monitoring intermode beats [3]. Today beating spectroscopy is an invaluable tool in many fields including quasi-elastic light scattering studies of macromolecules and critical phenomena of fluids [4], surface wave light scattering studies of the viscoelastic properties of fluid interfaces [5], and velocimetry of fluids [6,7]. In this paper we are mainly concerned with light scattering from interfacial fluctuations in fluids, in particular from capillary waves on liquid surfaces (also called ripples or ripplons) [8], which result from the interplay between thermal fluctuations and interfacial tension.

Consider a light beam striking the interface between two media with different indices of refraction. At a smooth and sharp interface, the beam is reflected and refracted. If the interface is rough, the incident light is scattered; if, in addition, the roughness is time-dependent, the scattered light has a different frequency spectrum from that of the incident light. Thus, by analyzing the spectrum of the light scattered from a fluctuating fluid interface, one can obtain information on the dynamics of the interface. The first attempts at measuring the capillary wave spectra of methanol and isopropanol were made by Katyl and Ingard using a Fabry-Pérot interferometer as a scanning optical filter [9]. Since the resolution of the interferometer was too low to resolve the capillary wave peaks, only a broadening of the incident light spectrum was observed. Using a differential light-beating technique, one year later, Katyl and Ingard were able to observe the capillary wave peaks of methanol [10]. At the same time Bouchiat et al. measured capillary wave spectra of ether and glycerine using a light-beating technique, and obtained the dispersion of the capillary waves [11,12]. Since then light-beating or heterodyne spectroscopy has been widely used to study capillary waves on a great variety of fluid interfaces [13–16].

The beat signal can be processed in the time domain to get an intensity correlation function or in the frequency domain to get the power spectrum. The intensity correlation function is typically obtained with an autocorrelator [17]; the power spectrum is obtained using a scanning electric filter [18], or by performing a Fourier transform on the intensity correlation function. One can also get the power spectrum more directly by performing a Fourier transform on the beat signal [17]. Recent advances in computer technology have made this frequency-domain analysis more convenient and cost-effective than conventional time-domain analysis using autocorrelators. Combined with a heterodyne detection

scheme this data analysis method is called Fourier-transform heterodyne spectroscopy [16].

In the next section we describe the relation between the scattered light and fluctuations in the scattering medium, and discuss the advantage of heterodyne detection with a frequency-shifted local oscillator. The experimental setup and the instrumental resolution limit of the technique are discussed next in Sects. 2 and 3. The final section presents two applications of the technique.

1 Optical correlations and hydrodynamic fluctuations

1.1 Measurement of light intensity

Consider a spatially coherent[1] light field described by a real electric field $E^R(t)$ of the form[2]

$$E^R(t) = \sum_m A_m^R(t)\cos[\Psi_m(t) - \omega_m t], \tag{1}$$

where $A_m^R(t)$ is a slowly varying real amplitude, and $\Psi_m(t)$ is the phase of the field for a positive angular frequency ω_m.[3] The associated complex electric field $E(t)$ is [20]

$$E(t) = \sum_m A_m(t)\,\mathrm{e}^{-\mathrm{i}\omega_m t}, \tag{2}$$

where

$$A_m t = A_m^R(t)\,\mathrm{e}^{\mathrm{i}\Psi_m(t)}. \tag{3}$$

The field in (1) is the real part of the complex field in (2),

$$E^R(t) = \mathrm{Re}\{E(t)\}. \tag{4}$$

The instantaneous intensity of the field $E^R(t)$ is then given by the magnitude of the Poynting vector

$$I(t) = c\varepsilon E^R(t)^2, \tag{5}$$

with c the speed of light, and ε the permittivity of the medium. The intensity measured by a detector is a time-average over the detector response time τ_d

$$\overline{I(t)} \equiv \frac{1}{\tau_d/2}\int_{-\tau_d/2}^{\tau/d} I(t+\tau)\,\mathrm{d}\tau. \tag{6}$$

In terms of the electric field, $\overline{I(t)}$ is given by

$$\overline{I(t)} = c\varepsilon\overline{E^R(t^2)} = \frac{c\varepsilon}{4}\sum_{mn}\Big[\overline{A_m(t)A_n(t)\,\mathrm{e}^{-\mathrm{i}(\omega_m+\omega_n)t}} + \overline{A_m^*(t)A_n^*(t)\,\mathrm{e}^{\mathrm{i}(\omega_m+\omega_n)t}} + 2\overline{A_m(t)A_n^*(t)\,\mathrm{e}^{-\mathrm{i}(\omega_m-\omega_n)t}}\Big]. \tag{7}$$

Since detector response times are much longer than the period of the electric field, we have

$$\overline{\mathrm{e}^{\pm\mathrm{i}(\omega_m+\omega_n)t}} = \frac{\sin[(\omega_m+\omega_n)\tau_d/2]}{(\omega_m+\omega_n)\tau d/2}\,\mathrm{e}^{\pm\mathrm{i}(\omega_m+\omega_n)t} \approx 0, \tag{8}$$

[1] The effect of spatial incoherence is discussed in [2].

[2] In this paper we are limiting ourselves to a classical treatment of the light field. For a quantum mechanical treatement see, e.g. [2,41].

[3] Throughout this paper we will use the frequency f and the corresponding angular frequency $\omega = 2\pi f$ interchangeably depending on which quantity is more appropriate in the context.

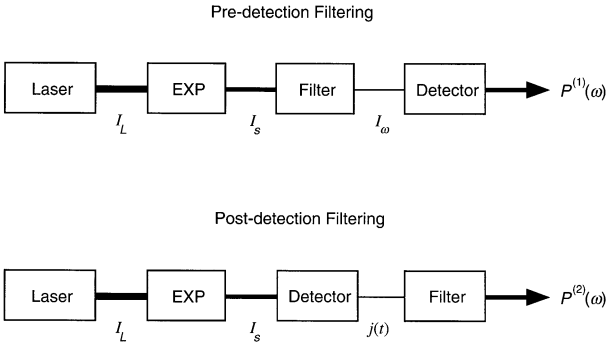

Fig. 1. Pre/Post-detection filtering. I_L and I_S are the intensities of the probing laser light and scattered signal, respectively; I_ω is the output mean power at ω with a bandwidth $\Delta\omega$; $j(t)$ is the detector current; $P^{(1)}(\omega)$ and $P^{(2)}\omega$ are the first- and second-order power spectrum, respectively

and the first and second terms in (7) can be neglected provided the amplitudes $A_m(t)$ are slowly varying functions of time. Therefore, in terms of the complex field the average intensity is given by

$$\overline{I(t)} = \frac{c\varepsilon}{2}\overline{E^*(t)E(t)}. \tag{9}$$

Note the subtile difference between (5) and (9). The more customary Equation (9) is valid only because in general detector response times far exceed the period of the optical field ($\tau_d \geq 1\times10^{-9}$ s; $2\pi\omega_m^{-1} \approx 1\times10^{-14}$ s).

1.2 Measurement of the frequency spectrum

Techniques for determining the frequency spectrum of scattered light fall into two categories [19]; pre-detection and post-detection filtering (Fig. 1). In the pre-detection filtering scheme one first spectrally filters the incident light, for example with a spectrometer or an interferometer, and then measures the intensity at a given frequency ω transmitted by the filter. This yields the optical or first-order power spectrum of the scattered field $E_s(t)$ [18]

$$P^{(1)}(\omega) \equiv \lim_{T\to\infty}\frac{1}{2T}|E_s(\omega)|^2, \tag{10}$$

where T is the sampling time and

$$E_s(\omega) = \int_{-\infty}^{\infty} E_s(t)\,\mathrm{e}^{\mathrm{i}\omega t}\,dt, \tag{11}$$

is the Fourier amplitude of the electric field component with angular frequency ω.

According to the Wiener-Khintchine theorem [18] the first-order power spectrum $P^{(1)}(\omega)$ is the Fourier transform of the first-order or *field* correlation function $G^{(1)}(\tau)$,

$$P^{(1)}\omega = \int_{-\infty}^{\infty} G^{(1)}(\tau)\,\mathrm{e}^{\mathrm{i}\omega\tau}\,d\tau, \tag{12}$$

where

$$G^{(1)}(\tau) \equiv \langle E_s^*(0)E_s(\tau)\rangle = \lim_{T\to\infty}\frac{1}{2T}\int_{-T}^{T} E_s^*(t)E_s(t+\tau)\,dt. \tag{13}$$

In the above equation we have used the ergodic theorem to replace the ensemble average by a time average [20].

In post-detection filtering the total intensity is first detected and the detector signal $j(t)$ is later filtered or processed to get the power spectrum of $j(t)$

$$P_j(\omega) \equiv \lim_{T\to\infty} \frac{1}{2T}|j(\omega)|^2, \tag{14}$$

where $j(\omega)$ is the Fourier transform of $j(t)$. Since the signal $j(t)$ is a real quantity, one has

$$\begin{aligned} P_j(\omega) &= \lim_{T\to\infty} \frac{1}{2T}\int_{-\infty}^{\infty} j(t)\,\mathrm{e}^{\mathrm{i}\omega t}\,dt \int_{-\infty}^{\infty} j(t')\,\mathrm{e}^{-\mathrm{i}\omega t'}\,dt' \\ &= \int_{-\infty}^{\infty} \langle j(0)j(\tau)\rangle\,\mathrm{e}^{\mathrm{i}\omega\tau}\,d\tau, \end{aligned} \tag{15}$$

which embodies the Wiener-Khintchine theorem. If the intensity of the light is large enough, the detector signal $j(t)$ is continuous and proportional to the average intensity $\overline{I(t)}$. The detector signal correlation function $< j(0)j(\tau) >$ is then proportional to the *intensity* correlation function

$$G^{(2)}(\tau) \equiv \left\langle \overline{I(0)}\,\overline{I(\tau)}\right\rangle = \lim_{T\to\infty}\frac{1}{2T}\int_{-T}^{T} \overline{I(t)}\,\overline{I(t+\tau)}\,dt. \tag{16}$$

Using the Wiener-Khintchine theorem and defining a second-order power spectrum in analogy to (10) we get

$$\begin{aligned} P_j(\omega) &\propto \int_{-\infty}^{\infty} G^{(2)}(\tau)\,\mathrm{e}^{\mathrm{i}\omega\tau}\,dt \\ &= \lim_{T\to\infty}\frac{1}{2T}|I(\omega)|^2 \equiv P^{(2)}(\omega). \end{aligned} \tag{17}$$

In other words, provided the signal is continuous, i.e., not in the photon counting regime, the power spectrum of the detector signal is proportional to the second-order power spectrum of the light.

1.3 Light scattering and spectral resolution

To compare the two techniques mentioned above, let us now consider more explicitly the case of a laser light scattering experiment. The incident monochromatic laser field is of the form

$$E_L(t) = A_L\,[1+\delta(t)]\,\mathrm{e}^{-\mathrm{i}\omega_L t+\mathrm{i}\Psi(t)}, \tag{18}$$

with ω_L the angular frequency of the light. A_L is the average field amplitude, $\delta(t)$ and $\Psi(t)$ are real, slowly varying random functions representing fluctuations in the amplitude and phase of the light, respectively [21]. We also assume

$$\langle\delta(t)\rangle = \langle\Psi(t)\rangle = 0, \tag{19}$$

$$|\delta(t)| \ll 1. \tag{20}$$

If fluctuations in a property $H(\mathbf{r},t)$ of the medium cause fluctuations in its electric susceptibility

$$\Delta\chi_{\mathbf{e}}(\mathbf{r},t) = \left(\frac{\partial\chi_e}{\partial H}\right)\Delta H(\mathbf{r},t), \tag{21}$$

the light will be scattered. The scattered field can be written in the form

$$E_s(t) = h_{\mathbf{q}}(t)[1+\delta(t)]\,\mathrm{e}^{\mathrm{i}\omega_L t+\mathrm{i}\Psi(t)}, \tag{22}$$

where $h_{\mathbf{q}}(t)$ is a stochastic complex quantity proportional to the fluctuations in the electric susceptibility $\Delta\chi_{\mathbf{eq}}(t)$ [7]

$$h_{\mathbf{q}}(t) \propto \Delta\chi_{\mathbf{eq}}(t) = \left(\frac{\partial\chi_e}{\partial H}\right)\Delta H_{\mathbf{q}}(t), \tag{23}$$

with $\Delta\chi_{e\mathbf{q}}(t)$ and $\Delta H_{\mathbf{q}}(t)$ the Fourier amplitudes of $\Delta\chi_e(\mathbf{r},t)$ and $\Delta H(\mathbf{r},t)$ for a fluctuation of wavevector $\mathbf{q}$, respectively. The subscript "$\mathbf{q}$" denotes the Fourier amplitude of a complex Fourier series expansion of a certain quantity. For instance, for a quantity $B(\mathbf{r})$ one has

$$B(\mathbf{r}) = \frac{1}{V}\sum_{\mathbf{q}} B_{\mathbf{q}} e^{\mathrm{i}\mathbf{q}\cdot\mathbf{r}}, \tag{24}$$

where V the volume of the system and

$$B_{\mathbf{q}} \equiv \int_V B(\mathbf{r})\,\mathrm{e}^{-\mathrm{i}\mathbf{q}\cdot\mathbf{r}}\,d\mathbf{r} \tag{25}$$

is the Fourier amplitude. In the limit $V\to\infty$, we may write the Fourier transform pair (24-25) as [22]

$$B(\mathbf{r}) = \int_{-\infty}^{\infty} B_{\mathbf{q}}\,\mathrm{e}^{\mathrm{i}\mathbf{q}\cdot\mathbf{r}}\frac{d\mathbf{q}}{(2\pi)^3}, \tag{26}$$

and

$$B_{\mathbf{q}} = \int_{-\infty}^{\infty} B(\mathbf{r})\,\mathrm{e}^{-\mathrm{i}\mathbf{q}\cdot\mathbf{r}}\,d\mathbf{r}. \tag{27}$$

Substituting the expression for the scattered light, (22 and 23), into (13), one gets

$$\begin{aligned} G^{(1)}(\tau) &= \langle E_s^*(0)E_s(\tau)\rangle \\ &\propto \langle\Delta H_{\mathbf{q}}^*(0)\Delta H_{\mathbf{q}}(\tau)\rangle\left\langle \mathrm{e}^{-\mathrm{i}\{\Psi(0)-\psi(\tau)\}}\right\rangle e^{-\mathrm{i}\omega_L\tau}, \end{aligned} \tag{28}$$

where the correlation functions of $\Delta H_{\mathbf{q}}(t)$ and $\mathrm{e}^{\mathrm{i}\Psi(t)}$ are separated since the laser source and the medium can be considered statistically independent of each other[4] and the small amplitude fluctuation $\delta(t)$ is neglected.

The spectrum of the scattered light is the Fourier transform of $G^{(1)}(\tau)$, see (12). As the second term on the right hand side of (28) shows, in pre-detection filtering the spectrum is in part determined by the phase fluctuations in the incident field. In particular, whenever the spectral width of the incident field is larger than the width associated with

[4] Consider a system having two independent parts, 1 and 2. Neglecting the interaction Hamiltonian between the two parts, we may write the Hamiltonian H_t and the distribution function f_t the entire system as

$$H_t(\Gamma_1\Gamma_2) = H_1(\Gamma_1) + H_2(\Gamma_2), \quad f_t(\Gamma_1\Gamma_2) = f_1(\Gamma_1)f_2(\Gamma_2),$$

where Γ_1, and Γ_2 are the coordinates of the phase spaces for the two parts; f_1 and f_2 are the corresponding distribution functions. Thus the average of any product $A(\Gamma_1)B(\Gamma_2)$ equals the product of the averages of A and B, since

$$\begin{aligned} \langle A(\Gamma_1)B(\Gamma_2)\rangle &= \int A(\Gamma_1)B(\Gamma_2)f_t(\Gamma_1\Gamma_2)\,d\Gamma_1\Gamma_2 \\ &= \int A(\Gamma_1)f_1(\Gamma_1)\,d\Gamma_1\int B(\Gamma_2)f_2(\Gamma_2)d\Gamma_2 \\ &= \langle A(\Gamma_1)\rangle\langle B(\Gamma_2)\rangle. \end{aligned}$$

the scattering process, the field correlation function of the scattered light and hence the optical power spectrum is dominated by the fluctuations in $\Psi(t)$. Another limiting factor for the spectral resolution is thefiltering process itself. To increase the frequency resolution, the passband width of the filter must be decreased and the transmitted signal intensity becomes correspondingly smaller. Thus the signal-to-noise ratio may limit the resolution even before the phase fluctuations play a role. In practice the limit of pre-detection filtering is on the order of a few MHz for interferometers [23].

Let us next consider post-detection filtering. The scattered light is now detected directly and the temporal behavior of the signal, caused by the beating of various spectral components of the scattered light, is analyzed according to (15). This scheme is called self-beating or homodyne[5] spectroscopy [24]. Substituting the expression of the scattered light, (22) and (23) into (16), one obtains the homodyne correlation function of the scattered light intensity $I_S(t)$

$$G_s^{(2)}(\tau) = \langle \overline{I_s(0)}\,\overline{I_s(\tau)} \rangle \propto \left\langle \overline{|\Delta H_{\mathbf{q}}(0)|^2}\,\overline{|\Delta H_{\mathbf{q}}(\tau)|^2} \right\rangle , \tag{29}$$

which is independent of the phase of the incident light. If the fluctuation $\Delta H_{\mathbf{q}}(t)$ is a Gaussian process [27], the homodyne correlation function is related to the correlation function of $\Delta H_{\mathbf{q}}(t)$ by

$$\left\langle \overline{|\Delta H_{\mathbf{q}}(0)|^2}\,\overline{|\Delta H_{\mathbf{q}}(\tau)|^2} \right\rangle = \left\langle \left|\overline{\Delta H_{\mathbf{q}}(0)}\right|^2 \right\rangle^2 + \left| \left\langle \overline{\Delta H_{\mathbf{q}}(0)}\;\overline{\Delta H_{\mathbf{q}}(\tau)} \right\rangle \right|^2 . \tag{30}$$

The first term on the right hand side gives rise to a delta function at zero frequency. When the correlation function $\langle \overline{\Delta H_{\mathbf{q}}(0)}\;\overline{\Delta H_{\mathbf{q}}(\tau)} \rangle$ is a simple exponential, the homodyne correlation function $G_s^{(2)}(\tau)$ is also a simple exponential and the power spectrum $P_s^{(2)}(\omega)$, which is the Fourier transform of $G_s^{(2)}(\tau)$, see (17), is a Lorentzian. For any other correlation function the power spectrum becomes complicated (7).

Note that the phase fluctuations in the incident field cancel out in the second-order power spectrum of the scattered light. The ultimate resolution is determined neither by the spectral width of the incident light source nor by the passband width of a filter but by the sampling time and the mechanical stability of the apparatus (Sect. 3).

1.4 Heterodyne detection

Although the homodyne technique has a high resolution, independent of the bandwidth of the light source, the intensity of the scattered light is often too small to overcome the detector noise. This problem can be solved by combining the scattered light with a coherent local oscillator signal and detecting the beat between the two [2]. In this heterodyne scheme the mixing of the local oscillator allows one to increase the signal level sufficiently so that the detector noise is negligible [26]. In addition, the frequency of the local oscillator can be shifted, allowing one to observe the spectrum near zero frequency [17].

For a general description of the heterodyne detection scheme, consider a local oscillator field coherent with the incident laser field with negligible delay[6] but frequency shifted by an amount $\Delta\omega_{LO}$ [7]

$$E_{LO}(t) = A_{LO}[1 + \delta(t)]\,\mathrm{e}^{-\mathrm{i}(\omega_L - \Delta\omega_{LO})t + \mathrm{i}\Psi(t)}. \tag{31}$$

At the detector this field is combined with the scattered light, E_s, see (22). Following (9), the intensity at the detector is then given by

$$\begin{aligned} \overline{I(t)} &= \frac{c\varepsilon}{2}\overline{|E_s(t) + E_{LO}(t)|^2} \\ &= \overline{I_s(t)} + \overline{I_{LO}(t)} \\ &\quad + \frac{c\varepsilon}{2}\left[\overline{E_s^*(t)E_{LO}(t)} + \overline{E_{LO}^*(t)E_s(t)}\right] . \end{aligned} \tag{32}$$

The product $\overline{I(t)}\,\overline{I(t+\tau)}$ has sixteen terms

$$\begin{aligned} \overline{I(t)}\;\; I(t+\tau) &= \overline{I_s(t)}\;\overline{I_s(t+\tau)} \\ &\quad + \overline{I_{LO(t)}}\;\overline{I_{LO}(t+\tau)} + \overline{I_s(t)}\;\overline{I_{LO}(t+\tau)} \\ &\quad + \overline{I_{LO}(t)}\;\overline{I_s(t+\tau)} \\ &\quad + \frac{c\varepsilon}{2}\left[\overline{I_s(t)} + \overline{I_{LO}(t)}\right]\left[\overline{E_s^*(t+\tau)E_{LO}(t+\tau)} + \text{c.c.}\right] \\ &\quad + \frac{c\varepsilon}{2}\left[\overline{E_s^*(t)E_{LO}(t)} + \text{c.c.}\right]\left[\overline{I_s(t+\tau)} + \overline{I_{LO}(t+\tau)}\right] \\ &\quad \frac{c^2\varepsilon^2}{4}\left[\overline{E_s^*(t)E_{LO}(t)}\;\overline{E_{LO}^*(t+\tau)E_S(t+\tau)} + \text{c.c.}\right] \\ &\quad + \frac{c^2\varepsilon^2}{4}\left[\overline{E_s^*(t)E_{LO}(t)}\;\overline{E_s^*(t+\tau)E_{LO}(t+\tau)} + \text{c.c.}\right] . \end{aligned} \tag{33}$$

If we take the time average of $\overline{I(t)}\,\overline{I(t+\tau)}$ to get the intensity correlation function (16), the ten terms containing factors of $\mathrm{e}^{-\mathrm{i}\omega t}$ vanish since

$$\lim_{\tau\to\infty} \frac{1}{2\tau}\int_{-\tau}^{\tau} B(t)\,\mathrm{e}^{-\mathrm{i}\omega t}\,dt = 0, \tag{34}$$

for any slowly varying function $B(t)$. If the amplitude of the local oscillator is larger than that of the scattered light

$$|A_{LO}| \gg |h_{\mathbf{q}}(t)|, \tag{35}$$

only the three largest time-dependent terms of the intensity correlation function remain:

$$\begin{aligned} G^{(2)}(\tau) &= \frac{c^2\varepsilon^2}{4}A_{LO}^2\left\{4A_{LO}^2\langle\delta(0)\delta(\tau)\rangle \right. \\ &\quad \left. + \left[\langle h_{\mathbf{q}}^*(0)h_{\mathbf{q}}(\tau)\rangle\,\mathrm{e}^{-\mathrm{i}\Delta\omega_{LO}\tau} + \text{c.c.}\right]\right\} . \end{aligned} \tag{36}$$

The first term in the right hand side of (36) is due to the fluctuations in the amplitude of the incident laser field. Its contribution can be either neglected if the resulting amplitude fluctuations of the local oscillator field are small enough to satisfy

$$|h_{\mathbf{q}}(t)| \gg |A_{LO}\delta(t)|, \tag{37}$$

[5] There are some differences in the use of 'homodyne' and 'heterodyne' in the literature. Here, self-beating of the scattered light by itself is referred to as *homodyne* detection, while the mixing of scattered light signal with a separate local oscillator is called *heterodyne* detection.

[6] The case of a local oscillator with non-negligible delay is discussed, for example, in [42].

[7] In the experiments described in this paper $\Delta\omega_{LO}$ is on the order of a few kHz.

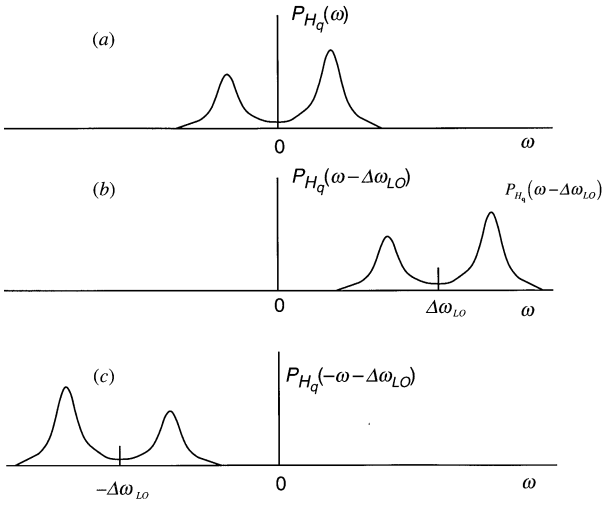

Fig. 2. Power spectra of hydrodynamic fluctuations in a quantity H; unshifted (a) and frequency-shifted (b and c), representing, respectively, the first and second terms in (41)

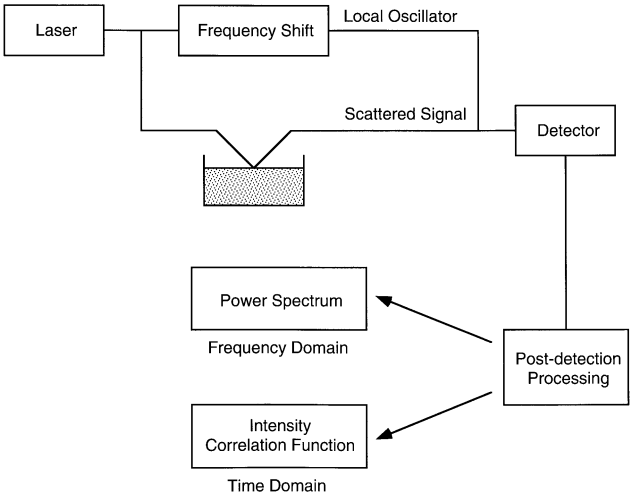

Fig. 3. Schematic diagram of a surface light scattering experiment

or calibrated by measuring the power spectrum of the laser separately Then the intensity correlation function and its power spectrum of the light at the detector reduce to

$$G^{(2)}(\tau) \propto \overline{I_{LO}} \left[\langle \Delta H^*_{\mathbf{q}}(0) \Delta H_{\mathbf{q}}(\tau) \rangle \, \mathrm{e}^{-\mathrm{i}\Delta\omega_{LO}\tau} + \text{c.c.} \right], \quad (38)$$

$$P^{(2)}(\omega) \propto \overline{I_{LO}} \left[P H_{\mathbf{q}}(\omega - \Delta\omega_{LO}) + P_{H_{\mathbf{q}}}(-\omega - \Delta\omega_{LO}) \right], \quad (39)$$

where $\overline{I_{LO}} = (c\varepsilon/2)\overline{|A_{LO}|^2}$ is the intensity of the local oscillator and $P_{H\mathbf{q}}(\omega)$ is the power spectrum of the hydrodynamic fluctuations in H for a particular wavevector $\mathbf{q}$,

$$P_{H_{\mathbf{q}}}(\omega) \equiv \lim_{T\to\infty} \frac{1}{2T} |\Delta H_{\mathbf{q}}(\omega)|^2 = \int_{-\infty}^{\infty} \langle \Delta H^*_{\mathbf{q}}(0) \Delta H_{\mathbf{q}}(\tau) \, \mathrm{e}^{\mathrm{i}\omega\tau} \, d\tau. \quad (40)$$

Combining (17 and 39), we finally see that the power spectrum of the detector signal is related to the power spectrum of the hydrodynamic fluctuations of the quantity H by

$$P_j(\omega) \propto \overline{I_{LO}} \left[P_{H_{\mathbf{q}}}(\omega - \Delta\omega_{LO}) + P_{H_{\mathbf{q}}}(-\omega - \Delta\omega_{LO}) \right]. \quad (41)$$

Note that (i) the phase fluctuations again cancel out in the intensity correlation function, provided the scattered light and the local oscillator fields are coherent, (ii) the signal level can be increased simply by increasing $\overline{I_{LO}}$, making detector noise negligible, and (iii) the relation between $P_j(\omega)$ and $P_{H_{\mathbf{q}}}(\omega)$ is much simpler than that for homodyne detection; in particular, it does not require the fluctuation $\Delta H_{\mathbf{q}}$ to be a Gaussian process, see (29 and 30).

If the local oscillator beam has the same frequency as the probing beam ($\Delta\omega_{LO} = 0$), the power spectrum of the detector signal of (39) becomes

$$P_j(\omega) \propto \left[P_{H_{\mathbf{q}}}(\omega) + P_{H_{\mathbf{q}}}(-\omega) \right], \quad (42)$$

which means that the power spectrum $P_{H\mathbf{q}}(\omega)$ for positive and negative frequencies are superimposed. When heterodyne spectroscopy is used to study equilibrium interfacial fluctuations, $P_{H\mathbf{q}}(\omega)$ is even in ω. Hence the power spectrum of the detector signal is directly proportional to the power spectrum of $\Delta H_{\mathbf{q}}$

$$P_j(\omega) \propto 2P_{H_{\mathbf{q}}}(\omega). \quad (43)$$

For a system out of equilibrium, however, this does not hold, because $P_{H\mathbf{q}}(\omega)$ and $P_{H\mathbf{q}}(-\omega)$ are different (Fig. 2) [29,30]. Usually the power spectrum $P_{H\mathbf{q}}(\omega)$ is bounded by a certain frequency range $\omega_{\max}$, such that $P_{H\mathbf{q}}\omega \approx O$ for $|\omega| > \omega_{\max}$. If the frequency shift $\Delta\omega_{LO}$ of the local oscillator is larger than the frequency range $\omega_{\max}$, the contribution of the term $P_{H\mathbf{q}}(-\omega - \Delta\omega_{LO})$ can be neglected for $\omega > 0$ and $P_j(\omega)$ is proportional to the spectrum of the hydrodynamic fluctuations $P_{H\mathbf{q}}(\omega)$ shifted by an amount $\Delta\omega_{LO}$

$$P_j(\omega) \propto P_{H_{\mathbf{q}}}(\omega - \Delta\omega_{LO}) \quad \text{for} \quad \omega > 0. \quad (44)$$

This is illustrated in Fig. 2b. The power spectrum is shifted away from zero frequency, out of the $1/f$ noise, so it becomes possible to observe $P_{H\mathbf{q}}(\omega)$ near zero frequency. In addition one can now distinguish between $P_{H\mathbf{q}}(\omega)$ and $P_{H\mathbf{q}}(-\omega)$.

2 Surface light scattering

In this section we discuss the application of this technique to the study interfacial hydrodynamic fluctuations. The general scheme of a heterodyne surface light scattering apparatus is shown in Fig. 3. Scattered laser light is combined with a local oscillator and the resulting beats are measured with a detector. The power spectrum of the beat signal can be shifted by changing the frequency of the local oscillator as in (44). To obtain efficient mixing of the local oscillator and the scattered light, it is essential that the two are coherent at the detector. Thus the optical path length of the local oscillator must equal the path length of the main beam. In addition, to ensure spatial coherence, the two beams must be carefully overlapped at the detector. We review here several techniques for the generation and frequency shifting of the local oscillator, and for the measurement of the beat signal spectrum.

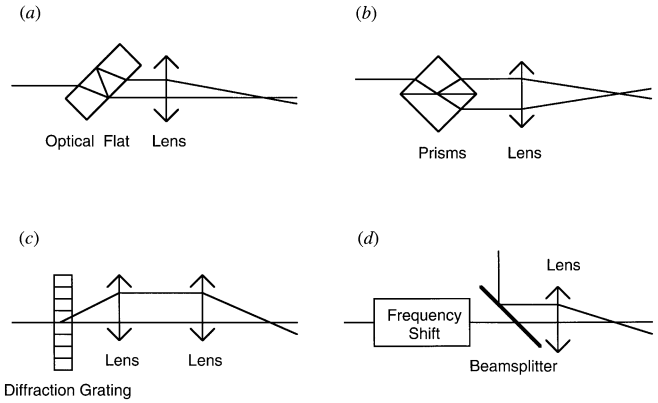

Fig. 4. Examples of parallel-beam methods. A pair of beams are made parallel by **a**) an optical flat, **b**) a prism pair [41], **c**) a diffraction grating and a lens, or **d**) a beam splitter. Then two beams are focussed onto a single probing point using a lens. The angle of convergence is determined by the focal length of the converging lens and the distance between the two parallel beams which can be changed by **a**) rotating the optical flat, **b**) translating the prism pair, **c**) using another diffraction grating and lens, or **d**) translating the beam splitter. Only method **d**) allows one to shift the frequency of the local oscillator beam

In early heterodyne experiments [29,30] the local oscillator was supplied by stray light scattered by impurities in the scattering volume or by optical elements near it. This method does not call for any alignment of the local oscillator, but makes it hard to control the intensity of the local oscillator and match it to the scattered light intensity. Nowadays the most widely used technique for creating a local oscillator involves the use of a diffraction grating [31,32]. While this technique allows one to control the intensity, one is limited to a fixed scattering angle determined by the ruling of the grating, and one cannot easily shift the frequency of the local oscillator.

Alternatively, one can generate a separate local oscillator beam using a beam splitter [17,33]. This allows one to control many properties of the local oscillator, such as its frequency, polarization, collimation, etc. There are several ways to recombine the local oscillator with the scattered light. One can either recombine the local oscillator with the scattered light using a second beam splitter, or cross the local oscillator and probe beams at the interface Recombining the two beams with a beam splitter is generally time consuming and difficult especially when the setup is floated by a pneumatic vibration isolation system. If a fiber optic directional coupler is used to combine the two beams, they are automatically superimposed, although residual table vibrations still limit the accuracy of the scattering angle on liquid interfaces.

If the local oscillator beam crosses the probe beam at the liquid interface at an angle θ it automatically overlaps with the light scattered at that angle. Since motion of the liquid interface changes the directions of both the scattered signal and local oscillator beams by the same amount without changing θ, the alignment is insensitive to interfacial motion. Furthermore, since one no longer needs a pinhole to select a scattering angle, the detector viewing angle can be made large enough to cover any movement of the beams resulting from interfacial motion. Figure 4 shows several optical arrangements that can be used for small scattering angles. In each case crossing is achieved by focussing two parallel beams at the interface. The last arrangement, (d), involving an entirely separate local oscillator, allows one to continuously vary the scattering angle θ by simple translation of a beamsplitter. Because of the separate beam path of the local oscillator and the main beam, one can also easily change the frequency, polarization, collimation, etc. of one or both of the beams.

As shown in the previous section one needs to shift the frequency of the local oscillator to separate the power spectra for negative and positive frequencies, see (44). This shifting of the local oscillator frequency has an additional advantage. Equation (32) shows that the beat signal contains a large dc component, $\overline{I_{LO}}$, which reduces the effective dynamic range of the detector signal. To remove this unwanted dc component one normally uses a high-pass electronic filter. However, this results in a distortion in the low frequency region of the spectrum. By changing the local oscillator frequency the entire power spectrum can be shifted out of this low frequency region, allowing one to study very low frequency fluctuations which would otherwise be filtered out. According to (44) these very low frequency fluctuations will be visible in the powerspectrum of the detector signal near the frequency shift $\Delta\omega_{LO}$ of the local oscillator. These advantages play an important role in the applications discussed in Sect. 4, which require a shift of only a few kHz. Generally the optimal frequency shift is determined by the spectral range of the particular application.

One way of shifting the frequency of a laser beam by a few kHz is to reflect it from a moving mirror. The Doppler shift of the reflected beam is

$$\Delta f = 2\frac{v}{\lambda}. \tag{45}$$

with v the longitudinal component of the velocity of the mirror, λ the wavelength of the beam. For a He-Ne laser (λ = 632.8 nm) a frequency shift Δf = 5 kHz requires a mirror speed of only 1.6 mm/s. For a typical coherence length of about 0.3 m for an unstabilized He-Ne laser this allows one to sample the detector signal up to 20 s in a single pass of the mirror. Although this method is simple and straightforward, it is limited by the steadiness and stability of the moving mechanism.

Another way of obtaining small frequency shifts is by acousto-optic modulation [17,34]. Acousto-optic modulators typically operate in the MHz frequency range,[8] which is much larger than the desired shift. For that reason, we use a scheme involving two slightly detuned modulators to generate a frequency shift in the kHz regime. The up-shifted component from the first modulator driven at a carrier frequency f_1 is used as an input to the second one driven at a carrier frequency f_2. The down-shifted component of the second modulator then has a resulting frequency shift

$$\Delta f_{LO} = f_2 - f_1. \tag{46}$$

Since the carrier frequencies f_1 and f_2 are in the radio-frequency range, Δf_{LO} can be controlled very accurately using standard crystal oscillators.

[8] At lower frequencies it is impossible to spatially separate the various frequency components of the light diffracted by the acousto-optic crystal.

The beat signal can be processed in the time domain to get an intensity correlation function or in the frequency domain to get the power spectrum. In early light beating experiments the power spectrum was obtained by scanning a narrow band electric filter over a magnetically recorded detector signal [35]. The resolution, determined by the bandwidth of the filter, was typically about 1 Hz. Later, autocorrelators were introduced which made it possible to measure the intensity correlation function, (29) directly. Autocorrelators make more efficient use of the signal than a scanning electric filter and provide the correlation function in real-time [36]. This technique also works well in the photon-counting regime. Furthermore, since the measured correlation function is a *product* of the instrumental function and the signal correlation function (in the case of a power spectrum it is a convolution), removing the instrumental contribution from the correlation function is mathematically easier. Because of these advantages, autocorrelators have become standard equipment in dynamic quasi-elastic light scattering experiments [7]. However, recent advances in computer technology have again rendered frequency domain analysis more practical. We have obtained excellent results using a personal computer equipped with an analog-to-digital converter board as a spectrum analyzer [17]. This computer-based method is versatile, convenient for data analysis, and, above all, very cost effective. In our experiment, the ac component of the photomultiplier signal is amplified and digitized by a GW Instruments MacAdios II computer board inside a Macintosh II computer. Then, the power spectrum of the detector signal is obtained by Fourier transforming the digitized waveform. The transform executed is a discrete fast Hartley transform, which is equivalent to a fast Fourier transform but requires only half the number of operations [37].

3 Experimental limits of Fourier transform heterodyne spectroscopy

3.1 Instrumental resolution

As we have seen the spectral resolution of heterodyne spectroscopy is not limited by fluctuations in the amplitude and phase of the light source. Factors that contribute to the instrumental resolution limit δf_{inst} are the finite sampling time, as well as electronic, mechanical, and optical instabilities.

The most fundamental limitation results from the finite sampling time, see (10). If the detector signal $j(t)$ is sampled for a period T (the sampling time), then the frequency interval δf_{samp} between adjacent spectral points in the Fourier transform of $j(t)$ is given by

$$\delta f_{\text{samp}} = \frac{1}{T}. \tag{47}$$

This resolution limit imposed by the sampling time can be made arbitrarily small by increasing the sampling time T. For a sampling time of four hours, δf_{samp} is 70 μHz which for a He-Ne laser corresponds to the Doppler shift that would result from the reflection of a mirror moving at a speed of 0.02 nm/s. In practice the instrumental resolution is determined by a convolution of limits due to electronic instabilities δf_e and to optical path length fluctuations δf_o

$$\delta f_{\text{inst}} = \delta f_e \oplus \delta f_o, \tag{48}$$

where $\oplus$ denotes the convolution of the two contributions.[9] These two resolution limits, δf_e and δf_o are considered in more detail below.

Fluctuations in the frequency shift Δf_{LO} of the local oscillator, δf_{LO}, and fluctuations in the digitization clock-rate δf_{clock} (Sect. 3.2), contribute to the electronic instabilities:

$$\delta f_e = \delta f_{LO} \oplus \delta f_{\text{clock}}. \tag{49}$$

Since the frequency shift Δf_{LO} is equal to the difference between the two rf carrier frequencies f_1 and f_2 for the two acousto-optic modulators, see (46), δf_{LO} is determined by the electronic drifts of the rf drivers for the acousto-optic crystals. One can easily get a carrier frequency stability of 100 Hz for a typical 40-MHz carrier frequency with a crystal oscillator; the frequency drifts of the crystal oscillator are mainly caused by temperature fluctuations. The stability of Δf_{LO} can be improved by either stabilizing the temperature of the separate crystal oscillators or by putting the two rf drivers into the same environment and letting them drift by the same amount. Using the latter method without temperature control of the crystal oscillators, we found that δf_{LO} was about 0.1 Hz by measuring the electronic beat signal of the rf outputs directly. This limit can be reduced further by locking the two crystal oscillators to a single oven-controlled time base; this way δf_{LO} could be further reduced down to 1 μHz.

Let us now turn to the second term in (48). In (22 and 31), we assumed the path lengths of the two beams are fixed. In reality, changes in the index of refraction of the air, mechanical perturbations of the optical elements due to temperature fluctuations, and acoustic noise cause optical path length fluctuations δf_o. For a temperature change of 1 K/hour, for example, a 1-m long optical path length contracts at a speed of about 0.25 nm/s because of changes in the index of refraction of the air. At the same time such a change in temperature would lead to a thermal expansion of the optical table of about 0.05 nm/s for a table made from carbon steel. Temperature fluctuations of 1 K/hour therefore would limit the resolution to about 300 μHz.[10] A rough estimate of the effect of a 100-Hz sound of 50 dB on a typical aluminum optical mount of 50-mm height and a square cross section of 10 $\times$ 10 mm^2 yields a lateral speed of the top surface of less than 0.01 nm/s, corresponding to a resolution limit resulting from acoustic noise δf_{noise} of about 30 μHz.

One should keep in mind, however, that the resolution limit is determined by the *difference* in Doppler shift of the local oscillator and signal beams, so the effective resolution limits δf_{temp} and δf_{noise} are generally much smaller than the above estimates. For the parallel-beam method (Fig. 4d), the local oscillator and signal beams have almost identi-

[9] For example, if these two contributions are Gaussian, the resulting resolution limit is given by

$$\delta f_{\text{inst}} = \sqrt{\delta f_e^2 + \delta f_o^2}.$$

[10] Note that the Doppler shift due to a decrease in optic al pathlength is one half of that in (45), since we are not dealing with a reflection here.

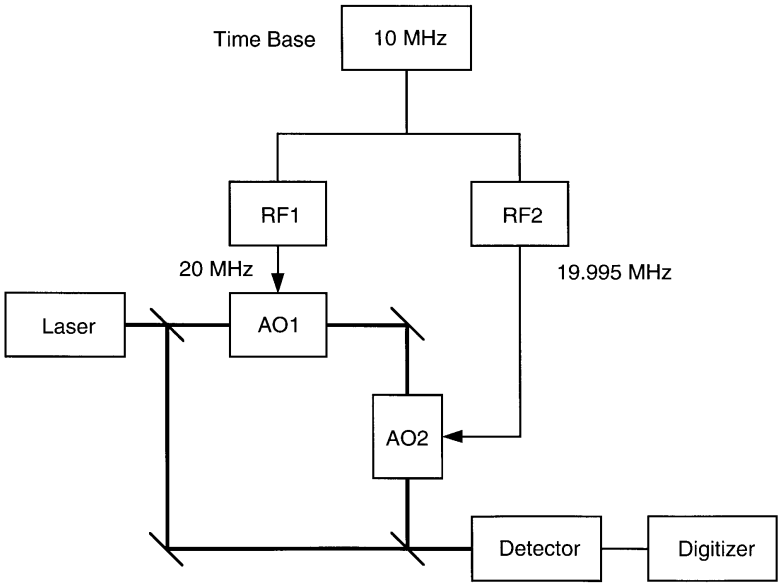

Fig. 5. Experimental setup for the measurement of the instrumental resolution using locked rf signals. AO1 and AO2 are two acousto-optic modulators. RF1 and RF2 are the two rf amplifiers for the acousto-optic modulators driven by two frequency synthesizers locked to a common time base

cal paths, so the resolution limit resulting from optical path length fluctuations is negligible for all practical purposes.

We determined the instrumental resolution δf_{inst} by mixing the local oscillator directly with the main laser beam as shown in Fig. 5, and investigated the contribution of the various terms in (48 and 49). The local oscillator was frequency-shifted using a combination of two acousto-optic modulators as described in the previous section. The two carrier frequencies of the modulators were in the 20–40 MHz range, with a frequency difference of 5 kHz.

The resolution was found to increase with increasing sampling time as expected from (47). When the two modulators were driven by two independent rf drivers (ME-40, IntraAction Corp.), a loss of resolution started to occur for sampling times longer than 60 s (open squares in Fig. 6). By comparing the FWHM of the 5-kHz peak in the optical beat spectrum with the one obtained by directly beating the two rf carrier signals, it was found that this loss of resolution was entirely caused by instabilities in the carrier frequencies (diagonal crosses). With two Hewlett-Packard 3325-B frequency synthesizers, locked to the same oven-controlled time base, the situation could be improved by a factor of one hundred. As can be seen in Fig. 6, the rf resolution follows (47) down to 140 μHz (vertical crosses). The optical resolution, on the other hand, starts to deviate from the theoretical value of (47) at about 400 μHz, most probably because of optical path length fluctuations of the setup during the half-hour sampling time. The highest instrumental resolution of the present setup (200 μHz), was obtained with a 4-hour sampling time.

3.2 Free spectral range and other considerations

If the detector signal $j(t)$ is sampled at a sampling frequency f_s (the inverse of the interval between adjacent sampling points, ΔT), then the spectrum, obtained by a discrete Fourier transform of the signal $j(t)$, has a free spectral range F given by[11]

$$F = \frac{1}{2\Delta T} = \frac{1}{2} f_s. \tag{50}$$

Generally, the upper limit of the free spectral range is determined either by the detector response time or by the speed of the signal digitizer; in practice, with a 1-ns detector response time and a fast transient digitizer, the free spectral range can be extended to the GHz regime. With a streak camera this could even be further extended by at least two orders of magnitude.

Because of the high, sub-mHz resolution and the large spectral range of several GHz, this technique is applicable to a wide variety of fields of research. The only other practical limit one needs to consider is the computation time required to analyze the detector signal. As one increases the number of data points, N, the time it takes to transform the data grows as $N \log_2 N$. The total number of data points is given by the product of the sampling time and the sampling frequency

$$N = T f_s \tag{51}$$

With a Macintosh II personal computer, the time needed to calculate the power spectrum of 2^{16} data points is about 40 s. However, this time can easily be reduced with faster computers. Table 1 summarizes various experimental aspects of the Fourier transform heterodyne technique.

[11] It is interesting to note here that the stability of the digitizer clock signal does not influence the resolution as much as that of the rf carrier frequencies. Fluctuations in the sampling rate due to clock signal instabilities lead to an uncertainty of the free spectral range in (50). If the total sampling time T is composed of N sampling intervals with an accuracy of a ($\ll 1$), the uncertainty of each point in the frequency spectrum is given by

$$\delta f_{\text{clock}} \approx \frac{\delta F}{N} \approx \text{a}\frac{f_s}{N} = \text{a}\frac{1}{T} = \text{a}\delta f_{\text{samp}}.$$

Therefore, δf_{clock} is much smaller than the sampling time limit, δf_{samp}, which cannot be avoided.

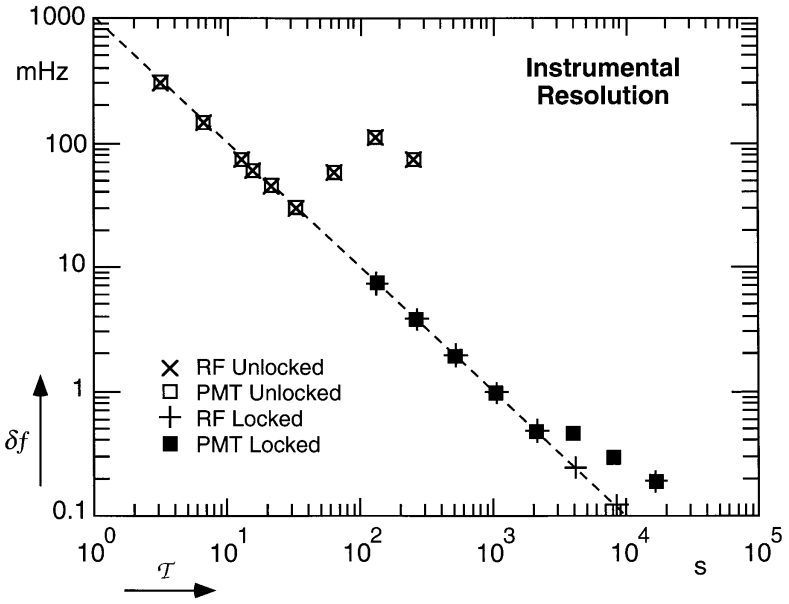

Fig. 6. Instrumental resolution as a function of sampling time. The crosses represent the FWHM (δf) of the central peak in the beat spectra of the two rf carrier signals; the squares represent those of the mixed beams at the photo-multiplier tube (PMT). The dotted line is the resolution limit due to finite sampling time given by (47)

Table 1. Experimental range and limitations of the Fourier transform heterodyne technique. Limiting factors and current limits of various contributions to the resolution limit are given. Spectral range and required computation time are also given

			Limiting factors	Current limit
Resolution limits	$\delta f_{\text{samp}} = \frac{1}{T}$		Sampling time (4 hours)	70 μHz
	δf_{inst}	δf_0 δf_{temp}	Temperature drift (1 K/hour)	$< 300\,\mu$Hz
		δf_{noise}	Acoustic noise	30 μHz
		δf_e δf_{LO}	Rf oscillator precision	1 μHz
		δf_{clock}	Clock accuracy (5×10^{-6})	0.2 nHz
Spectral range	$F = \frac{1}{2\Delta T} = \frac{N\delta f_{\text{samp}}}{2}$		Detector response time (< 1 ns)	> 1 Ghz
Computation time	$M \log_2 N,\ N = T f_s$		CPU/FPU ($N = 2^{16}$, Mac II)	40 s

4 Applications of Fourier transform heterodyne spectroscopy

4.1 Separation of counter-propagating capillary waves

The most important advantage of using a frequency-shifted local oscillator is the ability to shift the origin of the power spectrum. This enables one to study the asymmetric power spectrum of a system out of equilibrium [15]. To demonstrate this ability, we measured the power spectrum of capillary waves generated by an external force.

When a water surface is perturbed at a frequency f_{ind} by a transducer, a surface wave is generated which propagates away from the source. If the perturbation is strong enough, there will be a sharp peak in the power spectrum of the surface fluctuation either at frequency $+f_{\text{ind}}$ or $-f_{\text{ind}}$ depending on the direction of propagation of the surface wave. This can be made visible in a surface light scattering experiment. Consider a laser beam incident on the surface. Induced surfaces scatter the reflected light into two directions satisfying the conditions of conservation of energy and momentum in the plane of the surface [38].

$$(\mathbf{k}_{\text{scatt}})_{x,y} = (\mathbf{k}_{\text{laser}})_{x,y} \pm \mathbf{q}_{\text{ind}}, \tag{52}$$

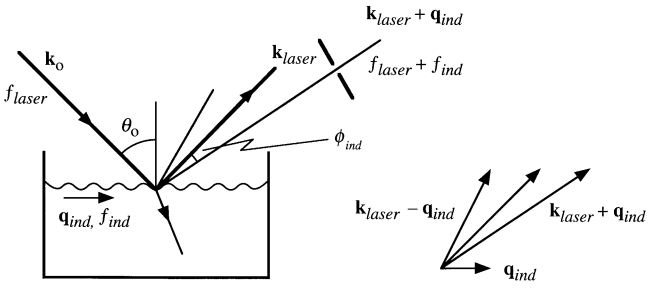

Fig. 7. Optical geometry for measuring the spectra of induced capillary waves. An incident light wave with wavevector $\mathbf{k}_0$, and frequency f_{laser} is reflected from the surface at an angle θ_0. The reflected light is scattered from a capillary wave with wavevector $\mathbf{q}_{\text{ind}}$ and frequency f_{ind}. The scattering angle ϕ_{ind} of the inelastically scattered light is determined by the phase-matching (momentum conservation) condition. Behind the pinhole the spectrum consists of a central peak at f_{laser}, and, for the capillary wave shown, a single capillary wave peak at $f_{\text{laser}} + f_{\text{ind}}$

$$f_{\text{scatt}} = f_{\text{laser}} \pm f_{\text{ind}}, \tag{53}$$

where $(\mathbf{k}_{\text{scatt}}, f_{\text{scatt}})$, $(\mathbf{k}_{\text{laser}}, f_{\text{laser}})$, and $(\mathbf{q}_{\text{ind}}, f_{\text{ind}})$ are the wavevectors and frequencies of the scattered light, reflected light, and induced surface wave, respectively (Fig. 7), and

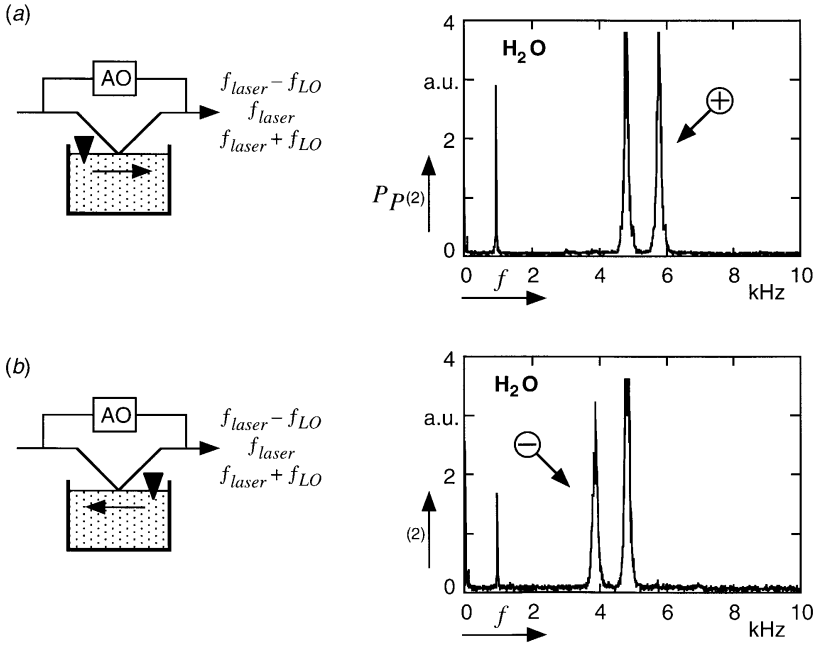

Fig. 8. Power spectra of induced capillary waves. A co-propagating **a**) or counter-propagating **b**) unidirectional capillary wave of frequency f_{ind} = 1 kHz is induced on the water surface by a transducer (black triangle) as shown in the diagrams on the left. In both cases the heterodyne spectrum shows only one capillary wave peak. The $\oplus$ and $\ominus$ signs show the peaks resulting from the beating of scattered light at $f_{\text{laser}} + f_{\text{ind}}$ and $f_{\text{laser}} - f_{\text{ind}}$, respectively. Note that the homodyne peaks, which correspond to the beating of the Rayleigh peak at $f_R (= f_{\text{laser}})$ with the capillary wave peaks at $f_{\text{laser}} \pm f_{\text{find}}$, appear at f_{ind}

the surface is in the xy-plane. The plus and minus signs correspond to annihilation and creation of a surface wave of wavevector $\mathbf{q}_{\text{ind}}$, respectively. The scattering angle ϕ_{ind} is given by the phasematching (momentum conservation) condition (52). Since $\mathbf{q}_{\text{ind}}$ is much smaller than $\mathbf{k}_{\text{laser}}$, the magnitudes of the incoming and scattered beams are approximately equal,

$$k_{\text{scatt}} \approx k_{\text{laser}}, \tag{54}$$

and one finds

$$\begin{aligned} q_{\text{ind}} &= k_{\text{laser}}[\sin(\theta_0 + \phi_{\text{ind}}) - \sin\theta_0] \\ &\approx \phi_{\text{ind}} k_{\text{laser}} \cos\theta_0, \end{aligned} \tag{55}$$

where θ_0 is the incidence angle.

For a surface wave of the same frequency f_{ind}, propagating in the opposite direction, (52 and 53) are modified as

$$(\mathbf{k}_{\text{scat}})_{x,y} = (\mathbf{k}_{\text{laser}})_{x,y} \pm \mathbf{q}', \tag{56}$$

$$f_{\text{scatt}} = f_{\text{laser}} \pm f_{\text{ind}}, \tag{57}$$

with

$$\mathbf{q}' = -\mathbf{q}_{\text{ind}}. \tag{58}$$

Therefore, for a given scattering angle, the frequency of the scattered light changes by an amount $\pm f_{\text{ind}}$ depending on the propagation direction of the surface wave. If an unshifted local oscillator is used in a surface light scattering experiment, however, the power spectrum of the detector signal will have a peak at the frequency $+f_{\text{ind}}$ regardless of the direction of propagation, see (41). If the local oscillator frequency is shifted by an amount Δf_{LO}, for a fixed scattering angle, the peak will appear either at $\Delta f_{LO} + f_{\text{ind}}$ or $\Delta f_{LO} - f_{\text{ind}}$ depending on the direction of propagation.

A wire attached to a speaker is used as a transducer to perturb the water surface. An electric signal of 1 kHz is supplied to the speaker to induce capillary waves at that frequency. For a given scattering geometry, the propagation direction of the induced capillary wave is reversed by changing the position of the transducer relative to the probing point. Spectra of counterpropagating capillary waves obtained with a 5-kHz frequency shift in the local oscillator are shown in Figs. 8a and b. A sharp peak appears at either 4 or 6 kHz depending on the direction of propagation and conservation of momentum, see (52 and 56). Additional peaks at 1 and 5 kHz correspond to the mixing of stray light with the scattered signal and local oscillator, respectively. These measurements clearly demonstrate the ability of the setup to separate counter-propagating capillary waves.

4.2 Epitaxial crystal-growth speed measurements

Because of its high resolution, one can use the Fourier transform heterodyne spectroscopy technique to observe very small frequency shifts. A possible application is the measurement of extremely small Doppler shifts. To illustrate this we have applied the technique to study solid phase epitaxial growth of silicon.

For an isolated piece of amorphous silicon, crystallization occurs through random formation of nucleation clusters and their subsequent growth. When an amorphous thin film of silicon is in direct contact with a crystalline substrate of silicon, the crystalline phase provides a template for ordered crystallization of the amorphous film. This occurs as a layer-by-layer conversion of silicon atoms from the amorphous to the crystalline phase. Since the index of refraction of amorphous silicon is different from that of crystalline silicon, a light beam will be reflected at the crystalline-amorphous silicon interface. One can obtain the growth speed of the interface by monitoring either (i) the interference between the reflected beam from the interface and the local oscillator beam using time-resolved reflectivity measurements [39, 40] or (ii) the Doppler shift of the reflected beam using Fourier transform heterodyne technique.

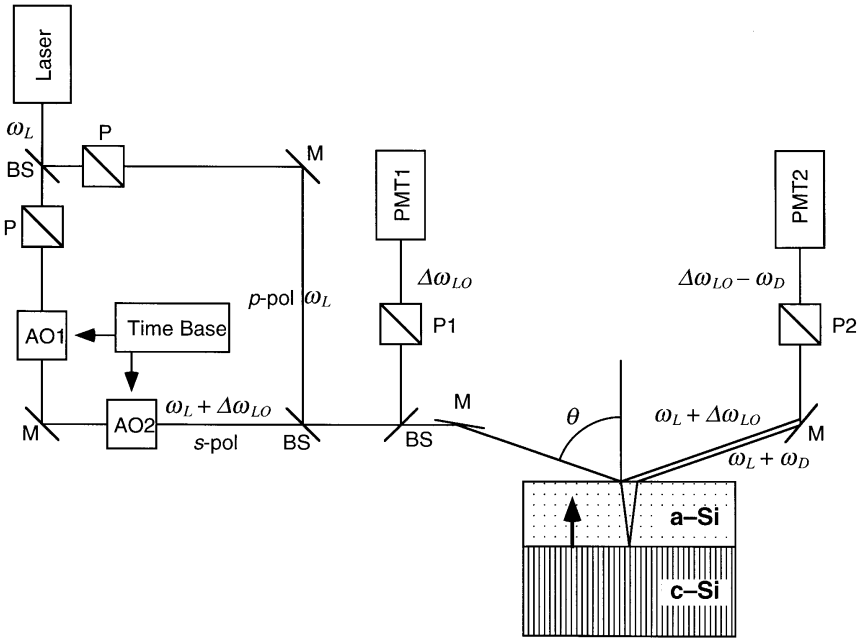

Fig. 9. Measurement of the Doppler shift ω_D from a growing amorphous/crystalline silicon interface. A p-polarized beam at angular frequency ω_L and an s-polarized beam at $\omega_L + \Delta\omega_{LO}$ are combined before they hit the interface at Brewster angle θ_0. PMT1 and PMT2 monitor the unshifted and Doppler-shifted peaks, respectively. (**M**: mirror; **BS**: beam splitter; **P**: polarizer; **PMT**: photomultiplier tube; **AO**: acousto-optic modulator)

The sample consists of a 200 μm $\times$ 200 μm substrate of crystalline silicon (100) covered with a 300-nm thick amorphous silicon layer made by implantation of $^{30}Si^{+}$. The silicon sample is placed on a heating unit in open air with the amorphous phase facing vertically upward. Since the silicon sample needs to be heated at 800 K or more to increase the crystal growth speed, high temperature air turbulence around the sample and reduced mechanical stability of the heater holding the sample greatly lower the overall stability of the setup. It is therefore necessary to mix the main laser beam with the local oscillator *before* hitting the sample to ensure constant overlapping of the two (Fig. 9). The main beam is incident at the Brewster angle to suppress reflection from the front air-amorphous silicon interface, which increases the mixing efficiency of the two specularly reflected beams. The Brewster angle is calculated using the real part of the index of refraction of amorphous silicon at the He-Ne laser wavelength of λ = 632.8 nm which is given by [39]

$$n_{\mathrm{a}} = 4.39 + 5 \times 10^{-4} T. \tag{59}$$

At 835 K, n_{a} = 4.81 and the Brewster angle, ignoring any contribution of the surface layer of silicon oxide, is given by

$$\theta_0 = \tan^{-1} n_{\mathrm{a}} = 78.2^{\circ}. \tag{60}$$

At this incidence angle the refraction angle is 11.7° and the change in the vertical component of the growth velocity is only 2% [= 1 − cos(11.7°)]. The main beam is p-polarized and the frequency-shifted local oscillator is s-polarized. Most of the local oscillator beam is reflected at the air-amorphous silicon interface, while most of the main beam penetrates the amorphous layer and is reflected at the crystalline-amorphous interface. Mixing of the two reflected beams is achieved by using a 45°-polarizer. The beat signals are sampled with two photomultiplier tubes. One photomultiplier tube (PMT1), monitoring the beat signal before the sample, provides a reference spectrum without a Doppler shifted peak. The Doppler shifted spectrum is obtained by another photomultiplier tube (PMT2). The pair of acousto-optic modulators (AOM-40, IntraAction Corp.) are driven at carrier frequencies of 20 000 and 20 005 MHz. These carrier signals are generated by two Hewlett-Packard 3325-B frequency synthesizers, locked to the same time base to stabilize the shifting frequency of the local oscillator beam.

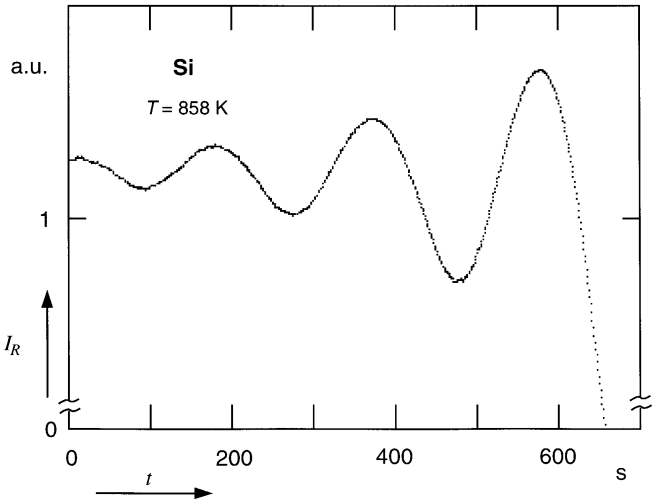

Fig. 10. Time-resolved reflectivity measurement of a growing amorphous/crystalline silicon interface at 858 K. The ratio of the outputs from the two PMT's, I_R, is monitored with time t

With the local oscillator beam blocked, the setup is identical to the standard time-resolved reflectivity measurement setup [39,40]. Figure 10 shows a trace of reflectivity as a function of time when the silicon sample is heated at 858 K. Since the film thickness increment between each successive interference maximum and minimum is $n_{\mathrm{a}}\lambda/4$, the growth speed can be obtained from this trace; this yields a growth speed of 0.35 nm/s in agreement with the published data of Olson and Roth [39].

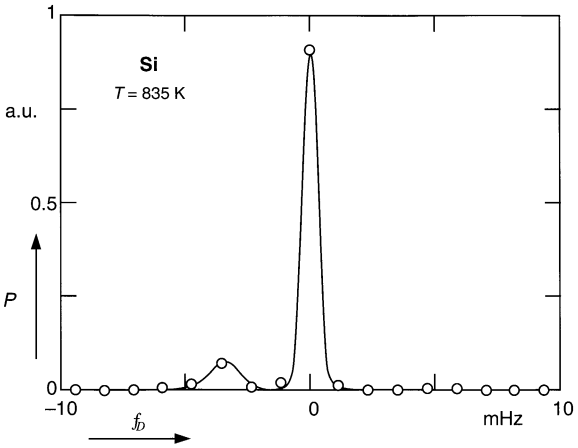

Fig. 11. Spectrum of the light reflected from a growing silicon crystal at 835 K. The small peak left of the large central one shows the Doppler shift due to crystal growth. The solid line through the data points is a guide to the eye

The spectrum of Fig. 11 was obtained with the shifted local oscillator beam unblocked. For this measurement the signal was sampled for 14 minutes at the rate of 76.9 Hz. Each point in the spectrum is 1.2 mHz apart. Circles are data points from the Fourier transform; the solid line is a guide to the eye. The large peak comes from the beating of the main beam and the local oscillator reflected at the air-amorphous silicon interface. The smaller peak is Doppler shifted by the motion of the crystalline-amorphous interface when the sample is heated at 835 K. The Doppler shift is 3 mHz, corresponding to a growth speed of about 0.2 nm/s. This is in good agreement with our time-resolved reflectivity measurements and published data [39].

In principle, by increasing the resolution, one could obtain the *distribution* of growth speeds over the sampled area from the broadening of the Doppler shifted peak (the shift reflects the *average* speed). The resolution of our measurements is limited by the maximum sampling time, which in turn is limited by the ratio of the amorphous layer thickness to the growth rate. For a fixed growth rate this means one needs thicker samples to increase resolution. However, since the amorphous silicon absorbs a significant amount of visible light, the useful thickness of the amorphous layer is also limited. The imaginary part of the index of the refraction of amorphous silicon, κ_a, is 0.61 at λ = 632.8 nm. For a 300-nm thick layer, 97 % of the light is absorbed (the absorption coefficient is $e^{-4\pi\kappa_a/\lambda}$). Thus, it is necessary to probe from the crystalline silicon side which has far less absorption (κ_s = 0.018) than the amorphous phase. Alternatively, the frequency of the light could be changed to reduce the absorption.

5 Conclusion

We have reviewed the theory of heterodyne spectroscopy and its application to surface light scattering. We also presented an improved version of the technique. Three distinct features of our apparatus are: a frequency shifted local oscillator, a phase-matched beam geometry, and a simple computer-based detection system. The frequency-shift of the local oscillator enables us to observe the full fluctuation spectrum of the medium. A frequency-shift of a few kHz can be achieved using a pair of acousto-optic modulators. By locking radio frequency signals for the two acoutso-optic modulators to a single time base, we achieved a resolution of 200 μHz. A major improvement in the versatility of the technique was achieved by aligning the signal and local oscillator beams in such a way as to automatically select scattered light of a given frequency. The benefits of this geometry are that one can continuously adjust the scattering wavevector and that the optical setup is much less sensitive to vibrations. Finally, we showed that the Fourier transform of the detector current gives the power spectrum of the scattering medium, free of the phase fluctuations of the light source. Recent advances in computer technology have rendered computer-based analysis of the signal feasible. The resulting detection and data-analysis system is versatile, convenient, and above all cost effective. Fourier transform heterodyne spectroscopy is an ideal technique for studying interfacial hydrodynamic fluctuations. As a demonstration of the directional sensitivity and high resolution of our apparatus, we presented measurements of counter-propagating capillary waves on a water surface, and of the epitaxial crystal-growth speed of a crystalline silicon interface, respectively.

Acknowledgements. The authors thank Prof. J.P. Wang and Mr. Aryeh Feder for valuable suggestions, and Prof. M.J. Aziz for the silicon sample and the temperature control unit. E.M. gratefully acknowledges support from the National Science Foundation (DMR-9400319). D.S.C. acknowledges grants from the Korean Ministry of Education Basic Sciences Research Institute (BSRI-96-3418) and the Korea Science and Engineering Foundation through the Center for Molecular Catalysis.

References

1. Forrester, A.T., Gudmundsen, R.A., Johnson, P.O.: Phys. Rev. **99**, 1691 (1955)
2. Cummins, H.Z., Swinney, H.L.: Prog. Opt. **8**, 133 (1970)
3. Forrester, A.T.: J. Opt. Soc. Am. **51**, 253 (1961)
4. Benedek, G.B.: In *Thermal Fluctuations and the Scattering of the Light*; ed. by M. Chetien, S. Deser, E.P. Gross (Gordon and Breach Science Publishers, New York 1968)
5. Loudon, R.: in *Ripples on Liquid Interfaces*, V.M. Agranovic, R. Loudon (North-Holland, Amsterdam 1984)
6. Yeh, Y., Cummins, H.Z.: Appl. Phys. Lett. **4**, 176 (1964)
7. Chu, B.: *Laser Light Scattering*, (Academic, New York 1974)
8. Landau, L.D., Lifshitz, E.M.: *Fluid Mechanics* (Addison-Wesley, Reading, MA 1959)
9. Katyl, R.H., Ingard, K.U.: Phys. Rev. Lett. **19**, 64 (1967)
10. Katyl, R.H., Ingard, K.U.: Phys. Rev. Lett. **20**, 248 (1968)
11. Bouchiat, M.A., Meunier, J.: C.R. Acad. Sci (Paris) B **266**, 301 (1968)
12. Bouchiat, M.A., Meunier, J., Brossel, J.: C.R. Acad. Sci. (Paris) B **266**, 255 (1968)
13. Earnshaw, J.C., McGivern, R.C., Winch, P.J.: J. Phys. France **49**, 1271 (1988)
14. Thominet, V., Stenvot, C., Langevin, D.: J. Colloid Interface Sci. **126**, 54 (1988)
15. Chung, D.S., Lee, K.Y., Mazur, E.: Phys. Lett. A **145**, 348 (1990)
16. Chung, D.S.: *Fourier Transform Heterodyne Spectroscopy of Liquid Interfaces*, Ph. D. thesis, Harvard University (1991)
17. Mazur, E., Chung, D.S.: Physica A **147**, 387 (1987)
18. Born, M., Wolf, E.: *Principles of Optics*, Pergamon, Oxford, (1975)
19. Brown, J.C.: Am. J. Phys. **51**, 1008 (1983)
20. Balescu, R.: *Equilibrium and Nonequilibrium Statistical Mechanics*, Wiley, New York, (1975)

21. Vahala, K., Yariv, A.: IEEE J. Quantum Electron. **QE-19**, 1096 (1983)
22. Bracewell, R.N.: *The Fourier Transform and Its Applications*, McGraw-Hill, New York 1965
23. Demtröder, W.: *Laser Spectroscopy*, Springer Berlin Heidelberg 1996
24. Ford, N.C., Benedek, G.B.: Phys. Rev. Lett. **15**, 649 (1965)
25. Mandel, L.: Prog. Opt. **2**, 181 (1963)
26. Jacobs, S.F.: Am. J. Phys. **56**, 235 (1988)
27. Grant, M., Desai, R.C.: Phys. Rev. **A 27**, 2577 (1983)
28. Desai, R., Grant, M.: in *Dynamics at a lipquid-vapor interface*, New York, C.A. Croxton (Wiley, 1986)
29. Lastovka, J.B., Benedek, G.B.: Phys. Rev. Lett. **17**, 1039 (1966)
30. Wu, E.S., Webb, W.W.: Phys. Rev. A **8** , 2077 (1973)
31. Hård, S., Hamnerius, Y., Nilson, O.: J. Appl. Phys. **47**, 2433 (1976)
32. Shih, L.B.: Rev. Sci. Instrum. **55**, 716 (1984)
33. Chung, D.S., Lee, K.Y.C., Mazur, E.: Int. J. Thermophysics **9**, 729–737 (1988)
34. Yariv, A.: *Quantum Electronics*. Wiley, New York (1989)
35. Cummins, H.Z., Knable, N., Yeh, Y.: Phys. Rev. Lett. **12**, 150 (1964)
36. Asch, R., Ford, N.C.: Rev. Sci. Instrum. **44**, 506 (1973)
37. Bracewell, R.N.: *The Hartley Transform* (Oxford Univ. Press, New York 1986)
38. Earnshaw, J.C.: in *Dynamics at a Liquid-Vapor Interface:* C.A. Croxton, Wiley, New York (1986)
39. Olson, G.L., Roth, J.A.: Mater. Sci. Reps. **3**, 1 (1988)
40. Lu, G.-Q.: *Pressure-Enhaced Crystallization Kinetics of Amorhous Si and Ge*, PhD thesis, Harvard University (1990)
41. Pike, E.R., Jakeman, E.: Adv. Quant. Electron. **2**, (1974)

This article was processed by the author using the LaTeX style file *pljour2* from Springer-Verlag.